Supporting Information

Spinodal-Modulated Solid Solution Delivers a Strong and Ductile Refractory High-Entropy Alloy

Zibing An[a], Shengcheng Mao*[a], Tao Yang[b], Chain Tsuan Liu[b], Bin Zhang[c], Evan Ma*[d], Hao Zhou[e], Ze Zhang[f], Lihua Wang[a], Xiaodong Han*[a]

Materials design

In terms of alloy design, we made our alloy using ductile elements, Hf, Ti, Nb, V, Zr and Ta.[1] Secondly, we desire adequate lattice distortions to ensure solid solution strengthening, so elements across a range of atomic size are selected. Third and more importantly, we aim to design spinodal decomposition of the parent BCC towards coherently interfaced BCC networks with different compositions and lattice strains. This possibility is inspired by the known phase separation in some Group IV-Group V (or Group IV-Group Ⅵ) binary systems. In such systems, a miscibility gap opens up over a range of temperature and composition, in which the BCC solid solution spinodally decomposes into (β+β*). Examples include Ti-Mo,[2] Zr-Nb[3] and Zr-Ta.[4] We therefore chose to experiment with a related system, the HfTi-VNb RHEA, and adjusted compositions to eventually land the alloy detailed in this paper.

Calculate the strengthening

In the HfNbTiV alloy, the yield strength is expected to have the contributions from frictional stress offered by the complex lattice to the mobile dislocations, strengthening due to the cocktail solid solution and spinodally decomposed modulations/interfaces. The yield strength, i.e. the flow resistance measured at the onset of plastic deformation,

is mainly achieved by solid solution strengthening in the alloy. The solid solution strengthening, can be regarded to originate from the elastic interactions between the local stress field of solute atoms and those of dislocations. However, in HEAs, it is hard to differentiate the solute and solvent elements. According to the Labusch approach,[5,6] the solid solution strengthening in BCC HEAs can be described as:

$$\Delta\sigma_{sssi} = ZGf_i^{\frac{4}{3}}C_i^{\frac{2}{3}} \qquad \text{(S1)}$$

where $\Delta\sigma_{sssi}$ is the increased strength by element *i*, *Z* is a fitting constant 0.04, *G*=56 GPa is the shear modulus of the alloy, obtained from nanoindentation measurements, C_i is the concentration of element *i* and the f_i parameter can be determined by:

$$f_i = \sqrt{\delta_{G_i}^2 + a^2\delta_{r_i}^2} \qquad \text{(S2)}$$

where δ_{G_i} is the atomic modulus mismatch and δ_{r_i} is the atomic size mismatch. The *a* is a constant, depending on the type of mobile dislocation (= 9 for a mixture of edge and screw dislocation).[7] For BCC HEAs, the δ_{G_i} and δ_{r_i} can be calculated as:

$$\delta_{G_i} = \frac{9}{8}\sum c_{j\delta_{G_{ij}}} \qquad \text{(S3)}$$

$$\delta_{r_i} = \frac{9}{8}\sum c_{j\delta_{r_{ij}}} \qquad \text{(S4)}$$

where c_j is the atomic fraction of j^{th} element in the alloy, $\delta_{G_{ij}} = 2(G_i - G_j)/(G_i + G_j)$, and $\delta_{r_{ij}} = 2(r_i - r_j)/(r_i + r_j)$. The solid solution strengthening is obtained by summation over $\Delta\sigma_i$ of each constituent via:

$$\Delta\sigma = (\sum \Delta\sigma_i^{3/2})^{2/3} \qquad \text{(S5)}$$

The atomic radii, valence electron concentration, shear moduli, and the yield strength of pure elements are given in Table S3. According to Equation (S1)-(S5), the calculated solid solution strengthening is 960 MPa. For the yield strength, "other strengthening

mechanisms", such as the interface between β and β* formed in spinodal decomposition, may contribute to the rest (1,100 – 960 = 140 MPa).

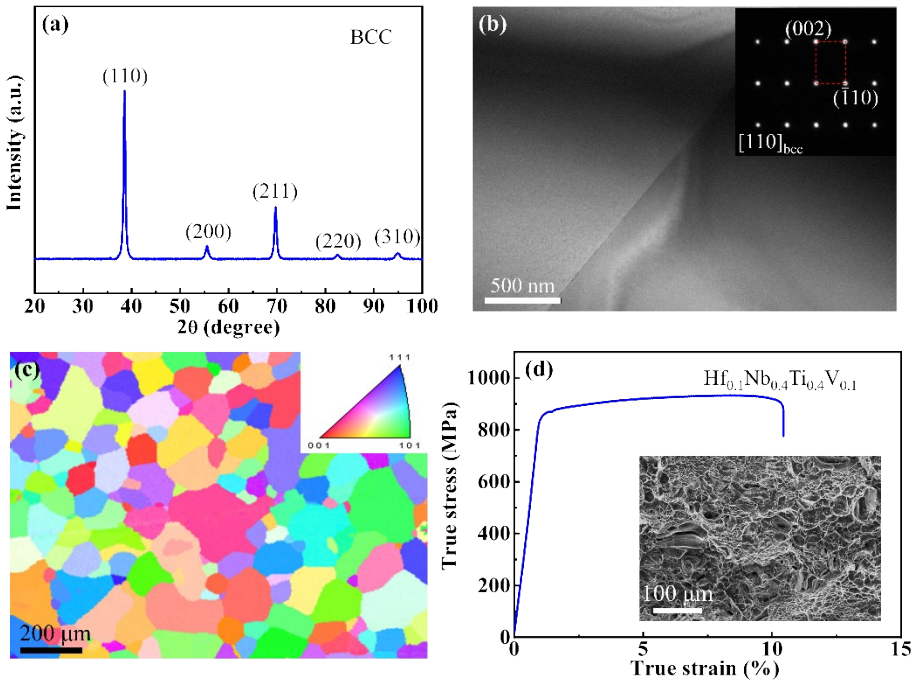

Fig. S1. The microstructure and tensile property of $Hf_{0.1}Nb_{0.4}Ti_{0.4}V_{0.1}$ alloy. (a) The XRD pattern of $Hf_{0.1}Nb_{0.4}Ti_{0.4}V_{0.1}$ alloy showing a single-phase BCC structure, (b) TEM bright field image and selected area electron diffraction patters show single-phase BCC structure, (c) Tri-color EBSD grain orientation map, (d) The true stress-strain curve of $Hf_{0.1}Nb_{0.4}Ti_{0.4}V_{0.1}$ alloy, the yield strength is 860 MPa and the tensile elongation is 10%.

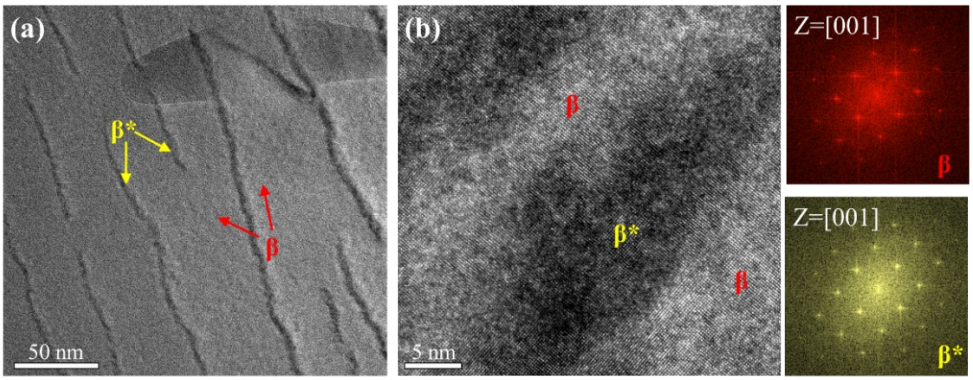

Fig. S2. Microstructure of the $Hf_{0.25}Nb_{0.25}Ti_{0.25}V_{0.25}$ alloy. (a) TEM image of $Hf_{0.25}Nb_{0.25}Ti_{0.25}V_{0.25}$ alloy, showing modulated β* and β. The β* is 50~300 nm in length and ~10 nm in width, (b) High-resolution transmission electron microscopy (HRTEM) image under [001] observed direction, the corresponding FFT patterns of the β and $β_*$ phase are shown in the right.

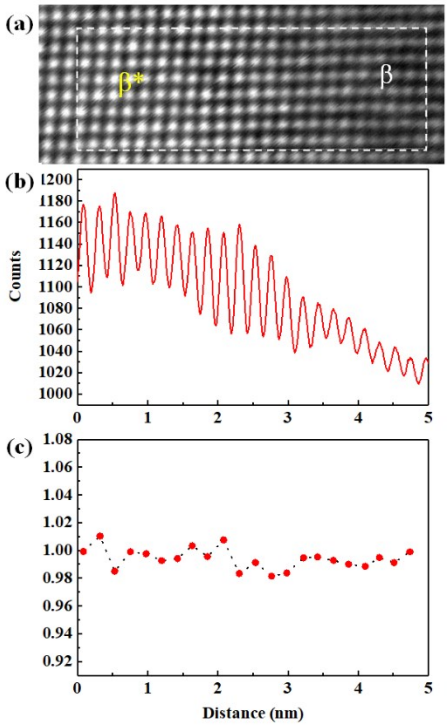

Fig. S3. The HAADF-STEM image of β* and β, showing gradual intensity change in the image. (a) HAADF-STEM image of the diffuse interface region between β* and β.

(b) Profile of intensity, averaged over the twenty-two columns in the vertical direction inside the box, plotted vs distance from the left side of the box to the right. The high intensity in β* indicates that it is enriched in higher Z elements, whereas β is richer in lower Z elements, (c) Intensity ratio of each atomic column to its adjacent column on the left.

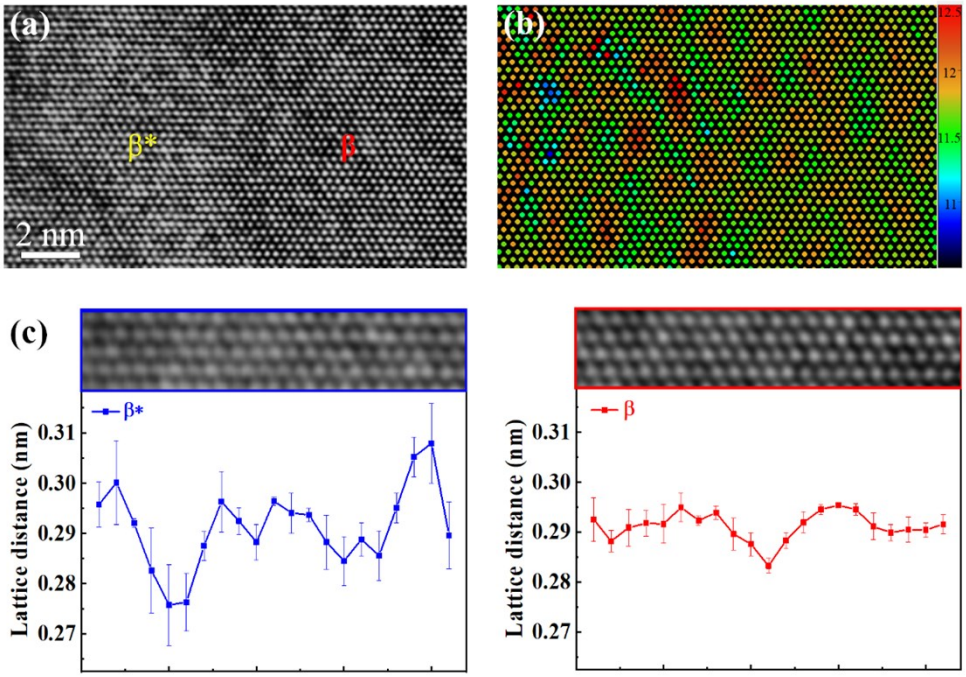

Fig. S4. Close-up view of the interfacial region between β* and β. (a) HAADF-STEM image, (b) Map of the interatomic spacing, measured for each atomic column relative to its neighboring column on the left. See color bar on the right for scale. Each pixel represents 0.025 nm, (c) The interatomic spacing measured in β* (left) and β (right).

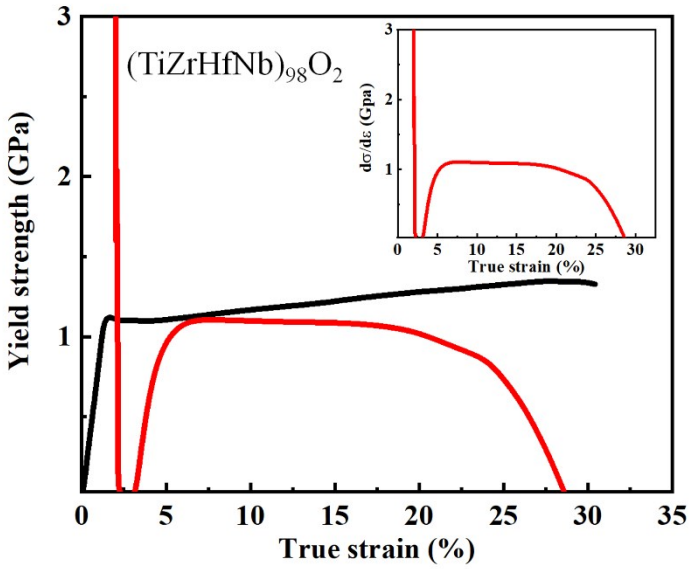

Fig. S5. Room-temperature tensile true stress–strain curves of the $(TiZrHfNb)_{98}O_2$ HEAs (O-2 alloy).[8] The inset shows the corresponding work-hardening response (dσ/dε), which drops rapidly early during plastic flow and is close to the flow stress only briefly, compare with Fig. 3(c).

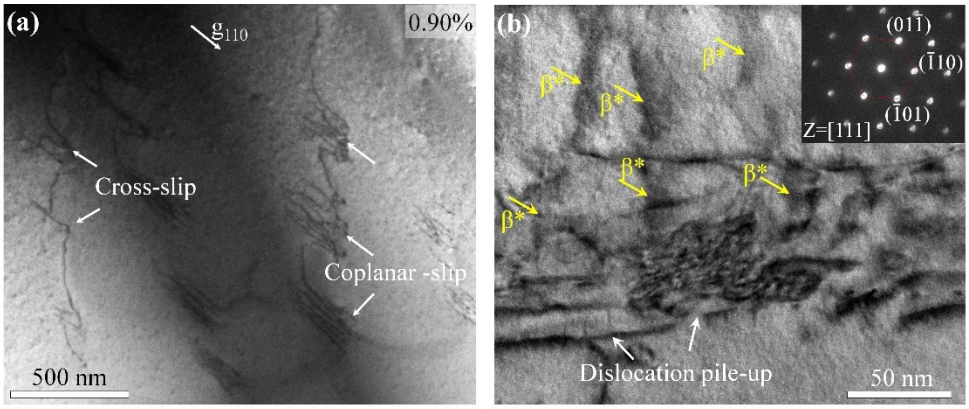

Fig. S6. Deformation mechanism of HfNbTiV alloy. (a) TEM image show coplanar slip of dislocations dominates in the early plastic deformation stage, with only occasional cross-slipped dislocations, after 0.9% strain. (b) TEM image showing the dislocations blocked by the β* (observed direction: [111]).

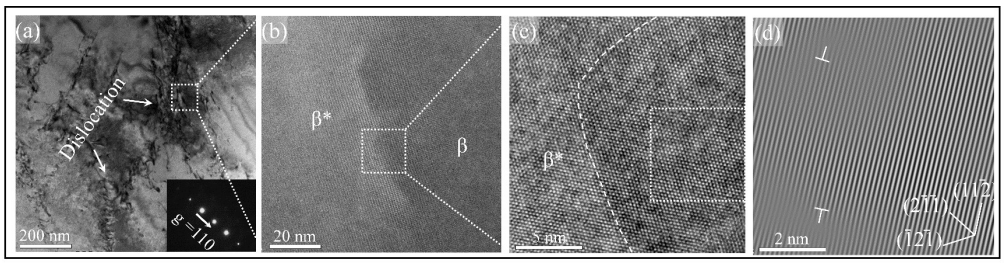

Fig. S7. Dislocations of HfNbTiV alloy. (a) Dislocations around a β* region, imaged under {111}-type diffraction conditions, and (b)-(d) Successive close-up HAADF-STEM images, viewed along [111] direction, showing details in the boxed region in the previous image. The edge components of dislocations are marked by "T" at dislocation cores.

Table S1. Chemical composition of the HfNbTiV alloy.

Element, at.%	phase	Hf	Nb	Ti	V
HfNbTiV	β*	29.6	21.4	21.1	27.9
	β	24.4	25.2	25.4	25.0

Table S2. The atomic radius (R), Valence electron concentration (VEC) and shear modulus (G) of constituent elements of HfNbTiV HEA.

Element	Ti	Hf	V	Nb
R (pm)	145	159	132	143
VEC	4	4	5	5
G (GPa)	45.6	56	46.6	37.5

Table S3. Local lattice strain in RHEAs.[9]

Composition	ε (%)
HfNbTaTiZr	0.91
HfNbTiZr	2.39
NbTiVZr	2.00
MoNbReTaTiVW	0.08
MoNbTaTiVW	0.21

MoNbReTaVW	0.23
MoNbReTaW	0.05
MoNbTaTiV	0.52
NbReTaTiV	0.02
MoNbTaV	0.65
MoNbTiV	0.01
NbReTaV	0.22
NbTaTiV	0.82
NbTaVW	0.32
HfNbTiV (this work)	5.00

References

1. L. Qi, D. C. Chrzan, Physical Review Letter, 2014, **112**, 115503.
2. C. Toher. S. Barzilai, S. Curtarolo and O. Levy, Physical Review Materials, 2017, **023604**, 8.
3. A. F. Guillermet, Ztschrift Fur Metallkunde, 1991, **82**, 478-487.
4. P. Zhou, Y. Peng, Y. Du, S. Wang, G. Wen, W. Xie and K. Chang, International Journal of Refractory Metals and Hard Materials, 2013, **41**, 408-415.
5. R. Labusch, Physica Status Solidi, 1970, **41**, 659-669.
6. R. L. Fleischer, Acta Metall, 1963, **11**, 203-209.
7. H. Yao, J. Qiao, J. A. Hawk, H. Zhou, M. Chen, M. Gao, Journal of Alloys and Compounds, 2017, **696**, 1139-1150.
8. Z. Lei, X. Liu, Y. Wu, H. Wang, S. Jiang, S. Wang, X. Hui, Y. Wu, B. Gault, P. Kontis, D. Raabe, L. Gu, Q. Zhang, H. Chen, H. Wang, J. Liu, K. An, Q. Zeng, T. G. Nieh and Z. Lu, Nature, 2018, **563**, 546-550.
9. Y. Tong, S. Zhao, H. Bei, T. Egami, Y. Zhang, F. Zhang, Acta Materialia, 2020, **183**, 172-181.